Turkish Journal of Chemistry

Volume 46 | Number 4 Article 21

1-1-2022

Detailed structure analyses on Cobalt doped PbTiO3 powders

EBRU ERÜNAL

Follow this and additional works at: https://journals.tubitak.gov.tr/chem

 Part of the Chemistry Commons

Recommended Citation

ERÜNAL, EBRU (2022) "Detailed structure analyses on Cobalt doped PbTiO3 powders," *Turkish Journal of Chemistry*: Vol. 46: No. 4, Article 21. https://doi.org/10.55730/1300-0527.3425
Available at: https://journals.tubitak.gov.tr/chem/vol46/iss4/21

This Article is brought to you for free and open access by TÜBİTAK Academic Journals. It has been accepted for inclusion in Turkish Journal of Chemistry by an authorized editor of TÜBİTAK Academic Journals. For more information, please contact academic.publications@tubitak.gov.tr.

Turkish Journal of Chemistry

http://journals.tubitak.gov.tr/chem/

Research Article

Turk J Chem
(2022) 46: 1176-1184
© TÜBİTAK
doi:10.55730/1300-0527.3425

Detailed structure analyses on Cobalt doped $PbTiO_3$ powders

Ebru ERÜNAL*
Department of Chemical Engineering, Çukurova University, Adana, Turkey

Received: 22.09.2021 • **Accepted/Published Online:** 08.04.2022 • **Final Version:** 05.08.2022

Abstract: The identification of the defects and secondary phases which significantly affect the material properties are of crucial importance. In this study, a systematic structure examination of $PbTiO_3$ and cobalt doped $PbTiO_3$ powder ceramics was carried out. X-ray diffraction (XRD), Fourier-transform infrared (FT-IR), Raman, and electron paramagnetic resonance (EPR) spectroscopies were applied along with nonsimultaneous thermogravimetric analysis (TGA) and differential scanning calorimetry (DSC). The doped and undoped $PbTiO_3$ materials were synthesized via a practical sol-gel route that takes place at 50 °C. The perovskite formation for both materials was verified. The dislocation density of cobalt doped $PbTiO_3$ was found to be 0.0121 nm^{-2} while it was 0.00239 nm^{-2} for the undoped material. Besides, a strong strain effect was observed for cobalt doped $PbTiO_3$ via XRD. This was attributed to the Co_3O_4 phase which was detected through EPR and FT-IR analyses. The formation of the Co_3O_4 phase during synthesis revealed the previously unexpected nonimproved ferroelectric behavior for cobalt doped $PbTiO_3$. The dielectric constant and the dielectric loss (tan δ) of cobalt doped $PbTiO_3$ were estimated as 1066 and 0.8370, respectively.

Key words: Co_3O_4, Doping, sol-gel synthesis, perovskite, $PbTiO_3$

1. Introduction

Today lead-based ferroelectric materials are still preferred in the industry due to their superior properties when compared with their alternatives [1–5]. Recently, there are even studies on the implementation of the spontaneous electric polarization of $PbTiO_3$ ceramics for photocatalytic applications to be used for the spatial separation of photogenerated electrons and holes [6,7]. In this context, the effect of doping should be well determined and carefully analyzed.

In general, the off-centered Ti^{4+} ions within the oxygen octahedra and other oxygen vacancies as a result of doping are attributed to the enhanced material properties [8]. One common mistake is the expected site of the dopant ion to be founded in such an ABO_3 type perovskite without considering its effective ionic radius. As a rule of thumb, ions with similar or closer effective ionic radii are more likely to change place with each other [9]. Therefore, if an ion is intended to dope on A site but has a closer effective ionic radius to the ion on B site, then there will be an excess of B site ions due to the wrong stoichiometric assumption. This will cause the formation of secondary phases. Moreover, synthesis routes would also end up with unwanted secondary phases which deteriorate the material properties instead of enhancement [10]. For example, cobalt doped $PbTiO_3$ would be expected to show distinct properties due to the magnetic character of the cobalt ion. However, Kumar et al. [11] reported no improvement in the ferroelectric properties of the cobalt doped $PbTiO_3$ which were obtained via sol-gel synthesis. The experimental observations are still not adequate to understand the reason for this phenomenon-whether result of secondary phases or changes in defect chemistry-. This study aimed to go further analysis of cobalt doped $PbTiO_3$ ceramics to enlighten the relation between the dielectric properties, the defects, and secondary phases obtained via sol-gel synthesis. In order to track the defect structure and secondary phases systematically, a comparative examination was carried out with the undoped $PbTiO_3$. When the effective ionic radius of dopant ion Co^{2+} (0.745 Å) is considered, it is expected to change place with Ti^{4+} ion whose effective ionic radius was reported as 0.605 Å [12]. For this reason, the precursor amounts were adjusted to obtain $Pb(Ti_{0.95}Co_{0.05})O_3$. The magnetic properties and the dielectric loss constant were interpreted with the detailed characterization results obtained through X-ray diffraction (XRD), Fourier transformation infrared (FT-IR) spectroscopy, Raman spectroscopy, thermal analyses, and electron paramagnetic resonance (EPR) spectroscopy.

* Correspondence: eerunal@cu.edu.tr

This work is licensed under a Creative Commons Attribution 4.0 International License.

2. Experimental

2.1. Materials

Lead(II) acetate trihydrate (extra pure, Merck), titanium isopropoxide (98%, Acros Organics), cobalt(II) nitrate hexahydrate (Carlo Erba), ethanol (absolute analytic, Merck), glacial acetic acid (Merck), and citric acid (%99, Sigma Aldrich) were used to obtain the undoped and cobalt doped $PbTiO_3$.

2.2. Sol-gel synthesis

The synthesis was carried out according to the method given by Odabasi [13]. Lead(II) acetate trihydrate ($Pb(CH_3COO)_2.3H_2O$) was dissolved in glacial acetic acid at room temperature. Appropriate dopant precursor (Co(II) $(NO_3)_2.6H_2O$ was also dissolved in this mixture. In another beaker, titanium isopropoxide ($Ti(OCH(CH_3)_2)_4$) was added to a mixture of glacial acetic acid and ethanol via a syringe. Two solutions were stirred at room temperature for around one h and then mixed. Vigorous stirring continued until a clear solution formed. Then, a mixture of citric acid and methanol was added to this solution. After a homogenous mixture was obtained, the temperature was raised up to 50 °C and heated for about one h. The cobalt doped material turned pink while the undoped material was off-white. All materials were calcined in two steps: Firstly, overnight at 100 °C and then at 650 °C for around three h with a heating rate of 50 °C/min.

3. Results and discussion

3.1. XRD analysis

The crystal structure was characterized with a Rigaku Miniflex XRD instrument (with a CuK_α, λ = 0.154 nm) between 20–80°. XRD patterns of both materials are given in Figure 1. The Miller indices of the main reflection planes (hkl) for $PbTiO_3$ perovskite structure are shown according to JCPDS card no. 01-077-2002. The perovskite structure with a tetragonal symmetry was obtained for both doped and undoped materials [14,15]. However, both homogenous and inhomogeneous strain effects are observed for the cobalt doped $PbTiO_3$. The slight shifts from peak positions for (001), (002), (201), (112) planes point out homogenous strain while the broadened peaks at 22–23°, 32–33°, 53°, and 56° show inhomogeneous strain. A similar inhomogeneous strain pattern was recorded by Elbasset et al. [16] for cobalt doped $PbTiO_3$ and interpreted as either grain size or local disorder effect. On contrary, the formation of a monoclinic $PbTi_3O_7$ phase (JCPDS card no. 00-021-0949), which was observed for the undoped $PbTiO_3$ around 28.9° and 34.6°, vanished upon cobalt doping [17,18]. Hence, the formation of this phase was also mentioned by Lee et al. [18] for $PbTiO_3$ powders synthesized via a similar sol-gel synthesis route. It was recorded that the formation of $PbTi_3O_7$ phase could be eliminated via calcination temperatures above 600 °C for more than three h.

The average crystallite sizes were estimated -with the help of Scherrer equation using (101) base peak- as 34.2 nm and 17.6 nm for undoped and cobalt doped $PbTiO_3$, respectively. The formation of defects as a result of cobalt doping may decrease the lattice parameters [19]. The lattice parameters were exploited from JPCDS Card Numbers via HighScore Plus software and compared with the calculated lattice parameters in Table. The difference between the expected (according to JCPDS Card Number) and calculated lattice parameters would result in phase transition temperature shifts like ±5 °C from Curie temperatures [10].

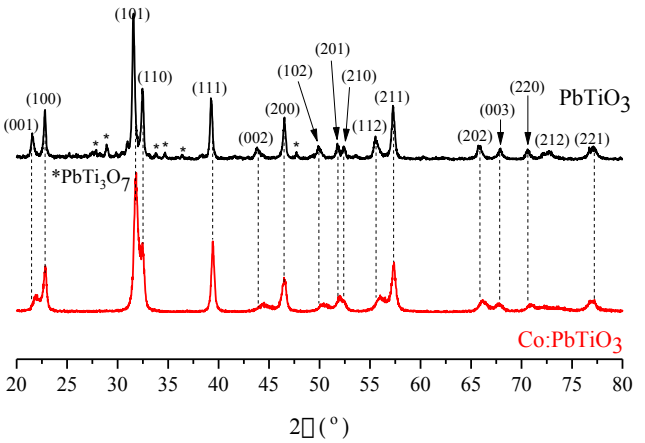

Figure 1. XRD patterns of $PbTiO_3$ (black line) and cobalt doped (red line) $PbTiO_3$ (red line) $PbTiO_3$

Table. Estimated lattice parameters for tetragonal symmetry.

Material	Lattice parameters (Å)				
	Database search			Calculated	
	JCPDS card number	a = b	c	a = b	c
$PbTiO_3$	01-077-2002	3.9000	4.1500	3.8953	4.1312
Co:$PbTiO_3$	01-078-0299	3.9400	4.0630	3.9005	4.0679

The dislocation densities were found as 2.39×10^{-3} nm^{-2} and 1.21×10^{-2} nm^{-2} for the undoped and cobalt doped $PbTiO_3$ with the help of the Williamson-Hall formula [20]. The very low dislocation density of the undoped $PbTiO_3$ is consistent with the similarly calculated lattice parameters. Moreover, the porosity of cobalt doped material was estimated. Bulk density (ρ_b) and X-ray density (ρ_x) were calculated as 4.504 g/cm^3 and 5.692 g/cm^3 according to the method given by Kumar et al. [11]. The porosity percentage (P%) was evaluated as 20% according to the following formula $P\% = [1- (\rho_b / \rho_x)] \times 100$.

3.2. Thermal analysis

Thermal analyses were carried out with a Mettler Toledo instrument under N_2 atmosphere with a flow rate of 40 mL/min. The thermogravimetric analyses (TGA) were carried out between 25 and 900 °C with a heating rate of 10 °C/min. The detailed TGA of cobalt doped $PbTiO_3$ was shown in Figure 2(a). In general, ceramics are quite stable at high temperatures [10]. As expected, the weight loss percentages were insignificant: 0.6% for undoped and 0.3% for cobalt doped $PbTiO_3$, as shown in Figure 2(a). It was already reported that $PbTiO_3$ ceramics decompose at temperatures higher than 900 °C [10]. Hence, PbO_x phases are decomposing between the measured temperature ranges [21]. The relatively higher weight loss of undoped $PbTiO_3$ was attributed to the decomposition of the PbO_2 phase to PbO with the help of the first derivative of thermogravimetric (DTG) data as demonstrated in Figure 2(b). Hence, the uncalcined secondary phases like PbO_2 start to decompose around between 250–350 °C and as temperature increases, PbO phase forms. For cobalt doped sample, even though PbO_2 was not detected, other PbO_x phases were identified [21]. Again, the decomposition of these phases ended up with PbO formation. The PbO_x-related secondary phases cause the formation of cation and oxygen defects even if they are in minor amounts since they affect the ratio of Pb/Ti ion stoichiometry slightly.

The differential scanning calorimetry (DSC) measurements were conducted between 25 and 550 °C with a heating rate of 8 °C/min again under N_2 atmosphere. The Curie temperature at which the tetragonal crystal structure changes to the cubic phase is expected at 490 °C for $PbTiO_3$ [10]. However, the detected Curie temperature was around 480 °C for the undoped $PbTiO_3$ in Figure 3. A difference of 10 °C from the expected Curie temperature value was attributed to a lead deficient ($V_{Pb}^{''}$) $PbTiO_3$ material [22]. The formation of PbO_x containing secondary phases would end up with such cation deficiencies within the perovskite structure. This will also cause the formation of oxygen vacancies ($V_O^{\cdot\cdot}$) in order to balance the crystal charge compensation [21,23]. By this way two negatively charged holes created by cation vacancy should be balanced with 2 plus charged oxygen vacancy as shown in Eqn (1) where $\oslash$ corresponds to the defect-free crystal structure.

$$V_{Pb}^{''} + V_O^{\cdot\cdot} \leftrightarrow \oslash \quad (1)$$

Apart from the undoped $PbTiO_3$, the Curie temperature vanishes for the cobalt doped $PbTiO_3$ in Figure 3. This phenomenon was also reported by Odabasi [13]. It might be related to the dislocation density that was estimated through the XRD analysis. The higher dislocation density may cause a decrease in detection limits for similar phase changes in the DSC analyses. Obviously, a counter exothermic peak at the expected Curie temperature is hindered as a result of cobalt doping. In order to resolve the spectrum, modulated DSC with a much slower heating rate should be applied [24]. Moreover, a bump between 150 and 250 °C followed by a sharp transition temperature around 305 °C was detected for the cobalt doped material. A similar trend at different temperatures was also observed for the undoped material. The bump of undoped and cobalt doped $PbTiO_3$ can be seen between 220 and 320 °C. The possible reason may be a Pb including secondary phase. The $PbTi_3O_7$ phase which was detected via XRD is known to be stable at these temperatures and decompose around 700 °C [18]. Another possibility is the pyrochlore ($Pb_2Ti_2O_6$) phase which was mentioned by Lee et al. [18]. Even though the XRD patterns of $Pb_2Ti_2O_6$ were hard to detect around 30°, in the DSC analysis, the sharp peaks at 315, 305, and 257 °C clearly point out the transformation of the pyrochlore phase to the tetragonal $PbTiO_3$ [18]. Because cobalt ion was also incorporated into this pyrochlore phase, a slight shift in the observed temperature was observed for cobalt doped $PbTiO_3$. Similar observations within the pyrochlore phase were reported for variously doped $PbTiO_3$ in literature [25–28].

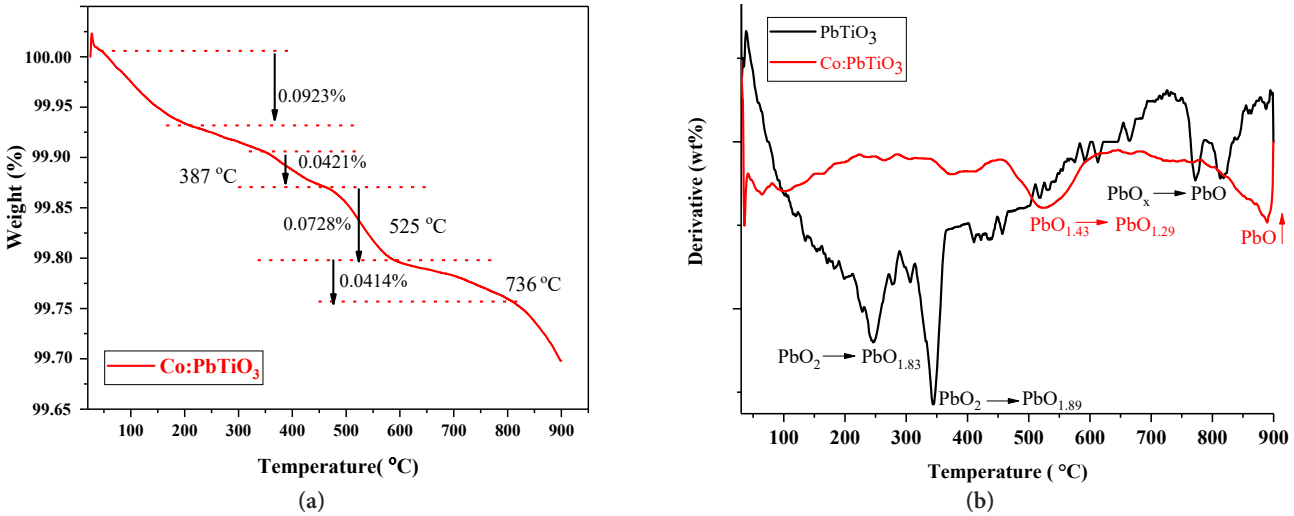

Figure 2. (a)TGA of cobalt doped $PbTiO_3$ **(b)** DTG of the undoped (black line) and cobalt doped (red line) $PbTiO_3$.

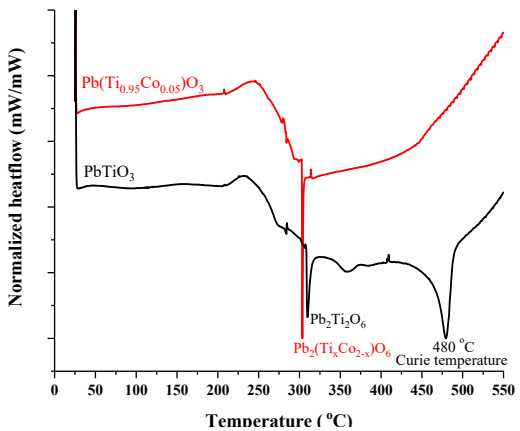

Figure 3. DSC measurements of undoped (black line) and cobalt doped (red line) $PbTiO_3$.

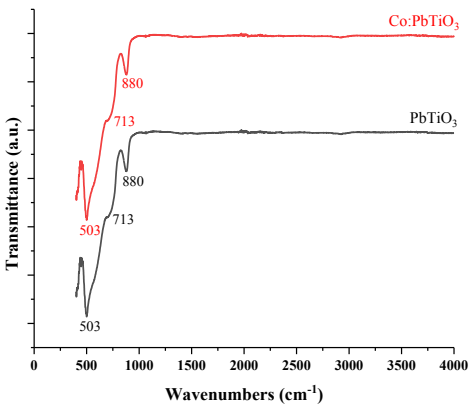

Figure 4. FT-IR spectra of undoped (black line) and cobalt doped (red line) $PbTiO_3$.

3.3 FT-IR measurements

The FT-IR measurements were conducted at room temperature, between 450 and 4000 cm^{-1} via an ATR crystal Thermo Scientific instrument. Two main peaks at 503 and 880 cm^{-1} for the undoped $PbTiO_3$ are seen in Figure 4. These peaks were associated with Ti–O and Pb–O bonds, respectively [29–31]. The slight bump around 713 cm^{-1}, which could also be detected for cobalt doped $PbTiO_3$, was attributed to six coordinated Ti^{4+} ion octahedral complexes within the perovskite structure [15]. Especially, the undoped and cobalt doped materials have quite similar spectra.

3.4 EPR spectroscopy

X-Band (9.7 GHz) EPR spectroscopy of doped materials was measured with a Bruker EMX 081 type EPR spectrometer at room temperature. Simply, EPR spectroscopy deals with the interaction of electromagnetic radiation with the molecule's dipole moment, which arises from an unpaired electron in its orbital [32–34]. Principally, each paramagnetic ion in a certain environment has a characteristic signal.

The Co^{2+} ion has three unpaired electrons in its high spin d^7 state. The spin Hamiltonian for high spin Co^{2+} is shown in Eqn.4 where β_e is the Bohr magneton, $\mathbf{B}_o$ is the applied external field, **g** is the g-factor or g tensor, **S** is the spin state, β_n is the nuclear magneton, $\mathbf{g}_n$ is the nuclear g-factor, **I** is the nuclear spin. **A** is the hyperfine interaction of the nucleus with the electronic spin and **D** is the zero-field splitting term that occurs from electron-electron dipole interaction of more than one unpaired electron containing system [33,34]. Since S is 3/2 and I is 7/2 for high spin Co^{2+} ion, splittings in its EPR spectrum are expected.

$$H = \beta_e \mathbf{B}_0 \cdot \mathbf{g} \cdot \mathbf{S} - \beta_n g_n \mathbf{B}_0 \cdot \mathbf{I} + \mathbf{S} \cdot \mathbf{D} \cdot \mathbf{S} + \mathbf{S} \cdot \mathbf{A} \cdot \mathbf{I} \quad (4)$$

Typical EPR spectrum examples for cobalt containing systems were given by Abragam & Bleaney and Telser [33,35]. Unfortunately, in Figure 5, the expected spectrum seems to vanish under the strong broad peak. A different measurement frequency rather than X Band may help to resolve this part.

In the literature, a similar broad peak was reported for Co_3O_4 [36] which is obtained through the calcination of CoO between 600 and 700 °C [37]. Apparently, CoO phase was formed during sol-gel synthesis and later turned into Co_3O_4 after calcination. This would result in less incorporation of Co^{2+} ions into the perovskite structure. Moreover, the broadenings in the XRD spectrum and thermal analyses of the cobalt doped material most likely arouse from this complicated secondary phase. However, it should be noted that the amount of this phase must be quite low and therefore below the detection limits of XRD, since during the analyses, the spectrum related to Co_3O_4 could not be exploited directly but just observed in terms of broadenings. Thus, Co_3O_4 has a spinel structure where Co^{3+} ions reside in the octahedral site, while Co^{2+} ions reside in the tetrahedral sites [37,38]. Normally, bulk Co_3O_4 was reported as antiferromagnetic at room temperature and Co_3O_4 nanoparticles were reported as magnetic only at very low temperatures [39]. Therefore, a magnetic susceptibility measurement was carried out to verify the incorporation of Co^{2+} ions into the perovskite structure. The magnetic susceptibility was compared with a copper doped $PbTiO_3$, which was synthesized with a similar route [28], and shown in Figure 6. A Vibrating Sample Magnetometer (VSM) system was utilized for magnetic measurements at room temperature. Even though both materials have low magnetic behavior, when compared with copper doped $PbTiO_3$, cobalt doped $PbTiO_3$ exhibits more ferromagnetic behavior. This may arise from the incorporation of cobalt ion into the $PbTiO_3$ perovskite structure. It should be noted that Co^{3+} in the Co_3O_4 phase was reported as diamagnetic due to its splitting in the spinel structure while the Co^{2+} ions have a small contribution to spin-orbit coupling. However, the magnetic susceptibility of the cobalt doped $PbTiO_3$ material was found to be higher than Co_3O_4 susceptibility as reported by Roth [38]. Therefore, this behavior was attributed to the incorporation of Co^{2+} within the targeted structure.

3.4. Raman spectroscopy

Raman spectroscopy was applied to verify the secondary phases detected through all other methods. It was conducted with an InVia Qontor model Renishaw instrument at room temperature. Typical $PbTiO_3$ phonon transitions [15,39–46] can be seen in Figure 7. After doping with cobalt, most of the transitions vanished or decreased drastically. The broadening of Raman lines and larger backgrounds for bulk ceramics were interpreted as an indication of disordered or amorphous structures [40].

Moreover, secondary phase-related transitions were found for both $PbTi_3O_7$ and Co_3O_4. For example, the modes around 129, 170, 252, 676, 749, and 836 cm^{-1} were corresponding to the $PbTi_3O_7$ phase [47], while the modes around 190, 474, 530, and 678 cm^{-1} were attributed to the Co_3O_4 phase [36,48].

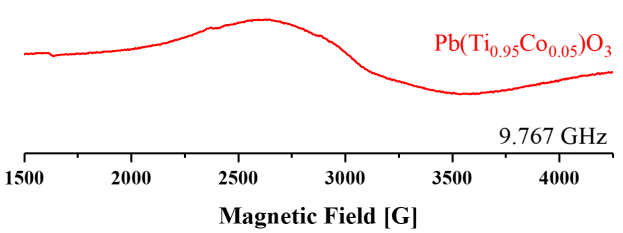

Figure 5. X-Band (9.767 GHz) EPR spectra of the cobalt doped $PbTiO_3$ measured at room temperature.

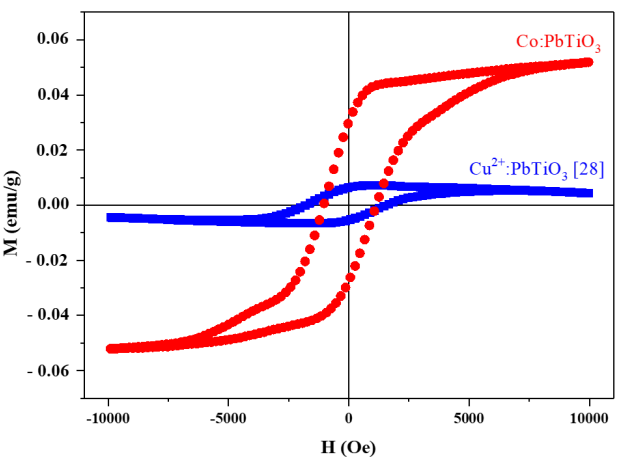

Figure 6. Comparison of the magnetic susceptibility measurements of cobalt (red) doped $PbTiO_3$ and copper (blue) doped $PbTiO_3$ [28] at room temperature.

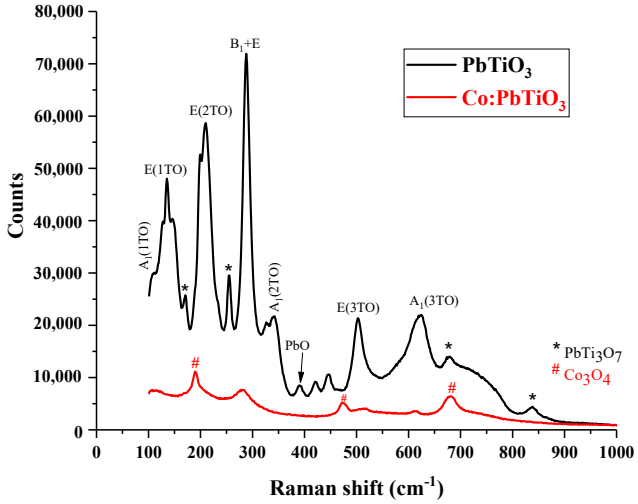

Figure 7. Raman spectra of undoped (black line) and cobalt doped (red line) $PbTiO_3$.

3.6. Dielectric properties

Cobalt doped $PbTiO_3$ pellets (0.6010 cm radius and 0.771 mm thickness) were obtained under 12 MPa pressure at room temperature and sintered at 700 °C for two h. Then, the surface of the pellets was coated with gold (Au) via vapor deposition (sputtering) technique before electrical measurements. The undoped material was not dense enough to obtain a proper pellet. Capacitance (C) and dielectric loss (tan δ) measurements of doped material were taken with an LCR-meter (INSTEK LCR-816) at a frequency of 1 kHz at room temperature. The capacitance (C) was measured as 1389 pF and relative permittivity (dielectric constant) was calculated as 1066. Dielectric loss (tan δ) was estimated as 0.8370. The dielectric loss at 1 kHz and dielectric constant were reported as 0.09 and 96.8 for the undoped $PbTiO_3$ capacitors [49]. The doping has affected the material's properties according to the increased values. Hence, the existence of pyrochlore phases at surfaces is known to decrease the dielectric constant. High dielectric constant value verifies the pyrochlore-free characterization results for cobalt doped material. Besides, the parameters obtained in this study are in good agreement with the literature for doped and composite $PbTiO_3$ based ceramics [10,50,51]. Co_3O_4 phase seems to enhance the dielectric constant. However, the existence of Co_3O_4 phase is thought to be the reason for not obtaining a proper polarization-electric field (P-E) loop hysteresis. The distorted banana shape shows a current leakage within the material. A similar P-E behavior was also observed by Kumar et al. [11]. It is obvious that the formation of CoO during sol-gel synthesis should be inhibited or this phase should be eliminated from the material before calcination so that Co_3O_4 phase can be avoided to overcome this problem.

4. Conclusions

The structural properties of the undoped and cobalt doped $PbTiO_3$ were investigated. Later these properties were used to interpret the nonferroelectric behavior of cobalt doped $PbTiO_3$. PbO_2, $PbTi_3O_7$, $Pb_2Ti_2O_6$ were detected for the undoped $PbTiO_3$, while slight PbO_x, $Pb_2(Ti_xCo_{2-x}O_6)$ formations were observed for cobalt doped $PbTiO_3$ through XRD, Raman and thermal analyses. Additionally, Co_3O_4 phase was detected through EPR and Raman spectroscopy. The vanishing Curie temperature of cobalt doped $PbTiO_3$ points out that a more sophisticated thermal analysis will be necessary to resolve the counter exothermic peak. The dielectric constant and dielectric loss for cobalt doped $PbTiO_3$ were estimated in good agreement with literature as 1066 and 0.8370, respectively.

Acknowledgments

This project is supported by Çukurova University Scientific Research Projects Coordination Unit (Project ID. FBA 2018-10647). Prof. Dr. Mustafa Polat from Hacettepe University, Prof. Dr. Ramazan Esen, and Prof. Dr. Bekir Özçelik from Çukurova University are acknowledged for their contributions to the EPR, XRD, and magnetic measurements. The Faculty of Science and Letters is acknowledged for the laboratory facilities. The author especially would like to thank Assist. Prof. Dr. Metin Özgül and Samet Abbak from Afyon Kocatepe University for dielectric and piezoelectric measurements provided. Dr. Klaus Seiffert, Oykun Gürkan, Umut Haskan, and H. Çağlar Üsdün are acknowledged for editorial assistance.

References

1. Gamboa B, Bhalla A, Guo R. Assessment of PZT (soft/hard) composites for energy harvesting. Ferroelectrics 2020; 555: 118-123. doi: 10.1080/00150193.2019.1691389
2. Song H-C, Kang C-Y, Yoon S-J, Jeong D-Y. Engineered domain configuration and piezoelectric energy harvesting in 0.7Pb(Mg1/3Nb2/3) O3-0.3PbTiO3 single crystals. Metals and Material International 2012; 18 (3): 499-503. doi: 10.1007/S12540-012-3018-Y
3. Priya S, Myers RD. Piezoelectric energy harvester, US7649305B2, 2010.
4. Hemeda OM, Eid MEA, Sharshar T, Ellabany HM, Henaish AMA. Synthesis of nanometer-sized PbZrxTi1-xO3 for gamma-ray attenuation. Journal of Physics and Chemistry of Solids 2021; 148: 109688. doi: 10.1016/j.jpcs.2020.109688
5. Eid MEA, Hemeda OM, Sharshar T, Ellabany HM, Weinstein I et al. Can nano PZT-OPC composites be used as a smart γ-ray attenuator? Journal of Physics and Chemistry of Solids 2021; 159: 110254. doi: 10.1016/j.jpcs.2021.110254
6. Liu Y, Ye S, Xie H, Zhu J, Shi Q et al. Internal-field-enhanced charge separation in a single-domain ferroelectric PbTiO3 photocatalyst. Advanced Materials 2020; 32 (7): 1906513. doi: 10.1002/adma.201906513
7. Zhu Q, Zhang K, Li D, Li N, Xu J et al. Polarization-enhanced photocatalytic activity in non-centrosymmetric materials based photocatalysis: A review. Chemical Engineering Journal 2021; 426: 131681. doi: 10.1016/j.cej.2021.131681
8. Angoshtari A, Yavari A. Effect of strain and oxygen vacancies on the structure of 180° ferroelectric domain walls in PbTiO3. Computational Material Science 2010; 48: 258-266. doi: 10.1016/j.commatsci.2010.01.006
9. Li G, Zheng L, Yin Q, Jiang B, Cao W. Microstructure and ferroelectric properties of MnO2-doped bismuth-layer (Ca, Sr)Bi4Ti4O15 ceramics. Journal of Applied Physics 2005; 98: 064108. doi: 10.1063/1.2058174
10. Jaffe B, Cook WR, Jaffe H. Piezoelectric ceramics. Academic Press, London, 1971.
11. Kumar NS, Suvarna RP, Naidu KCB. Structural and ferroelectric properties of microwave heated lead cobalt titanate nanoparticles synthesized by sol–gel technique. Journal of Materials Science: Materials in Electronics 2018; 29: 4738–4742. doi: 10.1007/s10854-017-8429-6
12. Shannon RD. Revised effective ionic radii and systematic studies of interatomic distances in halides and chaleogenides. Acta Crystallographica 1976; A32: 751-767. doi: 10.1107/S056773947600155
13. Odabaşı S. Effect of cobalt doping on photocatalytic activity of lead titanate. M.Sc. Thesis, M.E.T.U., Ankara, 2018.
14. Yang L, Wang Y, Wang X, Wang Y, Han G. Hydrothermal synthesis and characterization of PbTiO3 microrods. Advanced Material Research 2011; 149: 903–906.
15. doi: 10.4028/www.scientific.net/AMR.148-149.903
16. Ammar MH, El-hady MM, Salama TM, Bahgat AA. Reassess study of high temperature electric transport properties of PbTiO3. Journal of Alloys and Compounds 2019; 770 308-319. doi: 10.1016/j.jallcom.2018.08.113
17. Elbasset A, Lamcharfi T, Abdi F, Mrharrab L and Sayouri S. Effect of doping with cobalt or copper on the structure of lead titanate PT. Indian Journal of Science and Technology 2015; 8 (12): 1-6. doi: 10.17485/ijst/2015/v8i12/56348
18. Bersani D, Lottici PP, Montenero A, Pigoni S, Gnappi G. Phase transformations in sol-gel prepared PbTiO3. Journal of Material Science 1996; 31: 3153-3157. doi: 10.1007/BF00354661
19. Lee C-Y, Tai N-H, Sheu H-S, Chiu H-T, Hsieh SH. The formation of perovskite PbTiO3 powders by sol–gel process. Materials Chemistry and Physics 2006; 97: 468-471. doi: 10.1016/j.matchemphys.2005.08.048
20. Vinnik DA, Zherebtsov DA, Niewa R, Isaenko LI, Mikhailov GG. Distribution of dopant metals between PbTiO3 crystals and PbO–B2O3 flux. Russian Journal of General Chemistry 2014; 84: 1888–1892. doi: 10.1134/S107036321410003X
21. Williamson GK, Hall WH. X-ray line broadening from filed aluminium and wolfram. Acta Metallurgica 1953; 1: 22-31. doi: 10.1016/0001-6160(53)90006-6
22. Gavrichev K, Bolshakov A, Kondakov D, Khoroshilov A, Denisov S. Thermal transformations of lead oxides. Journal of Thermal Analysis and Calorimetry 2008; 92: 857-863. doi: 10.1007/s10973-007-8590-x
23. Peng X, Rong Y, Fan L, Lin K, Zhu H et al. Cation deficiency effect on negative thermal expansion of ferroelectric PbTiO3. Inorganic Chemistry Frontiers 2015; 2: 1091-1094. doi: 10.1039/C5QI00154D
24. Kröger FA, Vink HJ. Relations between the concentrations of imperfections in crystalline solids. Solid State Physics 1956; 3: 307-435. doi: 10.1016/S0081-1947(08)60135-6
25. Höhne GWH, Hemminger WF, Flammersheim H-J. Differential scanning calorimetry, 1st ed., Springer-Verlag, Berlin, 2003.
26. Lima Elton C, Araújo EB. Phase transformations in pzt thin films prepared by polymeric chemical method. Advances in Materials Physics and Chemistry 2012; 2: 178-184. doi: 10.4236/ampc.2012.23027

27. Kwok CK, Desu SB. Pyrochlore to perovskite phase transformation in sol-gel derived lead zirconate titanate thin films, Applied Physics Letters 1992; 60: 1430. doi: 10.1063/1.107312

28. Wang Y, Xu G, Yang L, Ren Z, Wei X et al. Preparation of single-crystal PbTiO3 nanorods by phase transformation from Pb2Ti2O6 nanorods. Journal of Alloys and Compounds 2009; 481: L27-L30. doi: 10.1016/j.jallcom.2009.03.073

29. Erünal E. Inhibition of secondary phase formation with minor copper doping on sol-gel derived PbTiO3 powders, Journal of Sol-Gel Science and Technology 2021; 101: 484-492. doi:

30. 10.1007/s10971-021-05700-0

31. Chauhan AKrS, Sreenivas K. TG-DTA and FT-IR studies on sol-gel derived Pb1-xCaxTiO3. Ferroelectrics 2005; 324: 77-81. doi: 10.1080/00150190500324659

32. Chaudhari VA, Bichil GK. Sol–gel synthesis and characterization of lead titanate films. Cogent Chemistry 2015; 1: 1075323. doi: 10.1080/23312009.2015.1075323

33. Toyoda M, Hamaji Y, Tomono K. Fabrication of PbTiO3 ceramic fibers by sol-gel processing. Journal of Sol-Gel Science and Technology 1997; 9: 71-84.

34. doi: 10.1023/A:1026464424392

35. Eichel R-A, Drahus MD, Jakes P, Erünal E, Erdem E et al. Defect structure and formation of defect complexes in Cu2+-modified metal oxides derived from a spin-Hamiltonian parameter analysis. Molecular Physics 2009; 107: 1981–1986. doi: 10.1080/00268970903084920

36. Abragam A, Bleaney B. Electron paramagnetic resonance of transition ions, Clarendon Press, London, 1970.

37. Weil JA, Bolton JR. Electron paramagnetic resonance–elementary theory and practical applications, 2nd ed., John Wiley & Sons, New Jersey, 2007.

38. Telser J. A perspective on applications of ligand-field analysis: inspiration from electron paramagnetic resonance spectroscopy of coordination complexes of transition metal ions. Journal of the Brazilian Chemical Society 2006; 17: 1501-1515.

39. doi: 10.1590/S0103-50532006000800005

40. Lou Y, Wang L, Zhang Y, Zhao Z, Zhang Z et al. The effects of Bi2O3 on the CO oxidation over Co3O4. Catalysis Today 2011; 175: 610-614. doi: 10.1016/j.cattod.2011.03.064

41. Greenwood NN, Earnshaw A. Chemistry of the elements, 2nd ed., Butterworth-Heinemann, Oxford, 1997.

42. Roth WL. The magnetic structure of Co3O4. Journal of Physical Chemistry of Solids 1964; 25: 1–10. doi: 10.1016/0022-3697(64)90156-8

43. Gawali SR, Gandhi AC, Gaikwad SS, Pant J, Chan T-S et al. Role of cobalt cations in short range antiferromagnetic Co3O4 nanoparticles: a thermal treatment approach to affecting phonon and magnetic properties. Scientific Reports 2018; 8: 249. doi: 10.1038/s41598-017-18563-9

44. Szafraniak-Wiza I, Hilczer B, Pietraszko A, Talik E. Phase formations during mechanochemical synthesis of PbTiO3. Journal of Electroceramics 2008; 20: 21-25. doi: 10.1007/s10832-007-9339-4

45. Burns G, Scott BA. Raman studies of underdamped soft modes in PbTiO3. Physical Review Letters 1970; 25: 167-170. doi: 10.1103/PhysRevLett.25.167

46. Meng JF, Katiyar RS, Zou GT. Grain size effect on ferroelectric phase transition in Pb1 – xBaxTiO3 ceramics. Journal of Physics and Chemistry of Solids 1998; 59: 1161-1167. doi: 10.1016/S0022-3697(97)00139-X

47. Hu Y, Gu H, Sun X, You Jing, and Wang J. Photoluminescence and raman scattering studies on PbTiO3 nanowires fabricated by hydrothermal method at low temperature. Applied Physics Letters 2006; 88: 193120. doi: 10.1063/1.2203736

48. Fontana MD, Idrissi H, Kugel GE, Wojcik K. Raman spectrum in PbTiO3 re-examined:dynamics of the soft phonon and the central peak. Journal of Physics: Condensed Matter 1991; 3: 8695-8705. doi: 10.1088/0953-8984/3/44/014

49. Bartasyte A, Margueron S, Santiso J, Hlinka J, Simon E et al. Domain structure and Raman modes in PbTiO3. Phase Transitions 2011; 84: 509–520. doi: 10.1080/01411594.2011.552433

50. Ma W, Zhang M, Lu Z. A study of size effects in PbTiO3 nanocrystals by raman spectroscopy. Physica Status Solidi a 1998; 166: 811-815. doi: 10.1002/(SICI)1521-396X(199804)166:2<811::AID-PSSA811>3.0.CO;2-X

51. Yahyaoui MM, Limame K, Sayouri S, Jaber B and Laanab L. Synthesis and structural studies of sol gel processed nanopowders of lead doped Y2Ti2O7 pyrochlores. Journal of Ceramic Processing Research 2017; 18: 252-260.

52. Zhao Q, Liu Q, Zheng Y, Han R, Song C et al. Enhanced catalytic performance for volatile organic compound oxidation over in-situ growth of MnOx on Co3O4 nanowire. Chemosphere 2020; 244: 125532. doi: 10.1016/j.chemosphere.2019.125532

53. Hsu M-C, Sun Y-M, Leu I-C, Hon M-H. Structural and electrical characterizations of PbTiO3 thin films grown on LaNiO3-buffered Pt/Ti/SiO2/Si substrates by liquid phase deposition. Journal of the Electrochemical Society 2006; 153 (11): F260-F265. doi: 10.1149/1.2349279

54. 50.Kwak JH, Han JK, Kang SW, Johnson TA, Bu SD. Dielectric relaxation properties of PbTiO3-multiwalled carbon nanotube composites prepared by a sol–gel process. Ceramics International 2016; 42 (7): 8165-8169. doi: 10.1016/j.ceramint.2016.02.023

55. Kumar NS, Suvarna KP, Naidu KCB. Sol-gel synthesized and microwave heated Pb0.8-yLayCo0.2TiO3 (y = 0.2–0.8) nanoparticles: Structural, morphological and dielectric properties. Ceramics International 2018; 44 (15): 18189-18199. doi: 10.1016/J.CERAMINT.2018.07.027